



# University of HUDDERSFIELD

## University of Huddersfield Repository

Elrawemi, Mohamed, Blunt, Liam, Fleming, Leigh, Bird, David, Robbins, David and Sweeney, Francis

Modelling water vapor permeability through atomic layer deposition coated photovoltaic barrier defects

### Original Citation

Elrawemi, Mohamed, Blunt, Liam, Fleming, Leigh, Bird, David, Robbins, David and Sweeney, Francis (2014) Modelling water vapor permeability through atomic layer deposition coated photovoltaic barrier defects. *Thin Solid Films*, 570A. pp. 101-106. ISSN 00406090

This version is available at <http://eprints.hud.ac.uk/id/eprint/21928/>

The University Repository is a digital collection of the research output of the University, available on Open Access. Copyright and Moral Rights for the items on this site are retained by the individual author and/or other copyright owners. Users may access full items free of charge; copies of full text items generally can be reproduced, displayed or performed and given to third parties in any format or medium for personal research or study, educational or not-for-profit purposes without prior permission or charge, provided:

- The authors, title and full bibliographic details is credited in any copy;
- A hyperlink and/or URL is included for the original metadata page; and
- The content is not changed in any way.

For more information, including our policy and submission procedure, please contact the Repository Team at: [E.mailbox@hud.ac.uk](mailto:E.mailbox@hud.ac.uk).

<http://eprints.hud.ac.uk/>



# Modelling water vapour permeability through atomic layer deposition coated photovoltaic barrier defects



Mohamed Elrawemi<sup>a,\*</sup>, Liam Blunt<sup>a</sup>, Leigh Fleming<sup>a</sup>, David Bird<sup>b</sup>, David Robbins<sup>b</sup>, Francis Sweeney<sup>a</sup>

<sup>a</sup> EPSRC Centre for Innovative Manufacturing in Advanced Metrology, School of Computing and Engineering, University of Huddersfield, Huddersfield, UK

<sup>b</sup> Centre for Process Innovation Limited, Sedgefield, County Durham, UK

## ARTICLE INFO

### Article history:

Received 11 March 2014

Received in revised form 26 August 2014

Accepted 29 August 2014

Available online 16 September 2014

### Keywords:

Defects

Permeation

Surface topography

Thin films

Water vapour transmission rate

## ABSTRACT

Transparent barrier films such as Al<sub>2</sub>O<sub>3</sub> used for prevention of oxygen and/or water vapour permeation are the subject of increasing research interest when used for the encapsulation of flexible photovoltaic modules. However, the existence of micro-scale defects in the barrier surface topography has been shown to have the potential to facilitate water vapour ingress, thereby reducing cell efficiency and causing internal electrical shorts. Previous work has shown that small defects ( $\leq 3 \mu\text{m}$  lateral dimension) were less significant in determining water vapour ingress. In contrast, larger defects ( $\geq 3 \mu\text{m}$  lateral dimension) seem to be more detrimental to the barrier functionality. Experimental results based on surface topography segmentation analysis and a model presented in this paper will be used to test the hypothesis that the major contributing defects to water vapour transmission rate are small numbers of large defects. The model highlighted in this study has the potential to be used for gaining a better understanding of photovoltaic module efficiency and performance.

© 2014 The Authors. Published by Elsevier B.V. This is an open access article under the CC BY-NC-ND license (<http://creativecommons.org/licenses/by-nc-nd/3.0/>).

## 1. Introduction

In today's industry, the most common type of solar photovoltaic (PV) cell is fabricated from either rigid crystalline silicon or thin-film materials [1]. The rigid construction of Si solar cells hampers their economic integration into residential and commercial buildings; however, thin film solar cell technologies may prove to be most appropriate with respect to cost, ease of manufacture and installation. These thin film cells are based on the material CuIn<sub>1-x</sub>Ga<sub>x</sub>Se<sub>2</sub> (CIGS) as the absorber layer (p-type) and they at present have efficiency levels at or beyond that of Si based rigid solar modules [2]. The key weakness of these cells however is their moisture sensitivity. This is a critical problem if this technology is expected to meet the requirements of international standard IEC61646 [3] which requires that all PV modules survive 1000 h in an environment of 85 °C and 85% relative humidity (RH) [3]. At the present time, no cost effective, flexible transparent encapsulation can fulfil the requirements of the water vapour transmission rate (WVTR) for flexible PV modules [4]. The WVTR of current barriers is in the range of 10<sup>-1</sup> g/m<sup>2</sup>/day, while it should not be higher than 10<sup>-4</sup> g/m<sup>2</sup>/day to assure life-times of 20 years and more [4,5].

Therefore, a robust, transparent flexible encapsulation method for flexible PV modules is needed.

Thin layers of aluminium-oxide (Al<sub>2</sub>O<sub>3</sub>) of the order of a few tens of nanometres deposited via the atomic layer deposition (ALD) technique have been introduced to allow PV module transparency and flexibility and to provide an effective barrier layer. These barrier films ideally have WVTR of less than 10<sup>-4</sup> g/m<sup>2</sup>/day [6]. The term 'barrier' here refers to the ability of Al<sub>2</sub>O<sub>3</sub> to resist the diffusion of water vapour into and through itself. Nevertheless, the barrier properties are often influenced by a wide range of variables, making conclusions regarding film properties sometimes difficult. It is known that barrier film permeability can be affected by the chemical and physical structures of the barrier, concentration of the permeant, temperature and humidity [7,8] as well as surface defects on the barrier coating that may be induced during the deposition processes [9,10]. Da Silva Sobrinho et al. [11] stated that the source of defect-driven permeation has been primarily attributed to pinhole defects [12,13] though more recent studies have shown that in the absence of pinhole defects permeation rates are still reduced by three orders of magnitude over the substrate material [14]. The remaining permeation is shown to be the result of defects in the sub-micrometre to several micrometre range, produced by the surface microstructure [15] and/or low density of the films [14–16]. More detailed reviews of permeation mechanisms and the performance of various permeation barriers have been given elsewhere [12,17]. In this paper a theoretical model is presented to allow the prediction of the amount of water vapour permeation through PV barrier film defects. The results of the model are then

\* Corresponding author at: EPSRC Centre for Innovative Manufacturing in Advanced Metrology, School of Computing and Engineering, University of Huddersfield, Huddersfield, HD1 3DH, UK.

E-mail addresses: [Mohamed.elrawemi@hud.ac.uk](mailto:Mohamed.elrawemi@hud.ac.uk), [elrawemi@yahoo.com](mailto:elrawemi@yahoo.com) (M. Elrawemi), [David.Bird@uk-cpi.com](mailto:David.Bird@uk-cpi.com) (D. Bird).

compared to experimental results where defects measured using surface metrology techniques are correlated with WVTR.

## 2. Theoretical model

Ashely [18] developed an equation to calculate the permeability coefficient of the water vapour through a polymer barrier film. The equation was based on Henry's law of solubility [19], Fick's laws of diffusion [20], Stefan and Exner's findings [21] and Von Wroblewski hypothesis [22]. Ashely [23] indicated that the permeability coefficient  $P_r$  depends on the solubility coefficient,  $S$ , as well as the diffusion coefficient,  $D$ . Eq. (1) expresses the permeability in terms of solubility and diffusivity,  $D$ , and it can be defined as the volume of vapour passing through a unit area of the barrier layer per unit time, with a unit pressure difference across the sample [23].

$$P_r = \frac{(\text{quantity of permeant}) \times (\text{film thickness})}{(\text{area}) \times (\text{time}) \times (\text{pressure drop across the film})}$$

$$P_r = DS = \frac{qL}{At\Delta P} \left( \frac{\text{cm}^3 \text{cm}}{\text{cm}^2 \cdot \text{s} \cdot \text{Pa}} \right) \quad (1)$$

where  $q$  is the amount of permeant passing through a film of thickness  $L$  and over area  $A$  during time  $t$  driven by a partial pressure differential  $\Delta P$  across the film [24]. In a typical water vapour permeation measurement, for example, a "MOCON" test,  $\Delta P$  in Eq. (1) corresponds to the partial pressure difference between nitrogen containing water vapour at 90% RH on one side, and ultra-pure nitrogen on the other side. In this type of permeation test there is no pressure gradient across the sample so it is then reasonable to use the absolute value of the permeant's partial pressure  $P$ , instead of  $\Delta P$  [11]. Thus, Eq. (2) can be presented as the following;

$$P_r = DS = \frac{qL}{AtP} \left( \frac{\text{cm}^3 \text{cm}}{\text{cm}^2 \cdot \text{s} \cdot \text{Pa}} \right). \quad (2)$$

Da Silva Sobrinho et al. [11] developed an equation to determine the amount of permeant per unit of time ( $Q$ ) through the polymer; this equation was based on Henry's law of solubility [19]. This equation is mathematically expressed as;

$$Q = \frac{q}{t} = \frac{ADSP}{L} = \frac{AD\emptyset}{L} \quad (3)$$

where the validity of Henry's law is assumed, and  $\emptyset$  represents the water vapour concentration in the film surface and it has been estimated to be  $1 \text{ g/cm}^3$  [11]. For the case of water vapour which has a little [25] or even no interaction with the barrier film [11,26], the water vapour transmission is completely governed by defect geometries and densities [11]. In the present paper a model of water vapour permeation through the barrier defects is presented to study the effect of the defects on water vapour permeation.

### 2.1. Single defect case

The basic assumption is that the combined film of thickness  $L$  is made up of a transparent flexible barrier coating of ( $\text{Al}_2\text{O}_3$ ) with a single circular hole (defect) of radius ( $R_0$ ), and that it is exposed to permeant water vapour from the lower side as shown in Fig. 1.

Considering only steady-state permeation, where temperature and partial pressure of the water vapour are constant, and the total pressure is the same on both sides of the barrier layer. The next step is to determine the amount of the water vapour  $q_H$ , leaving the barrier film, see Fig. 1. In steady state, this amount is clearly determined by the water passing through the defect in the barrier. However, in the case of the

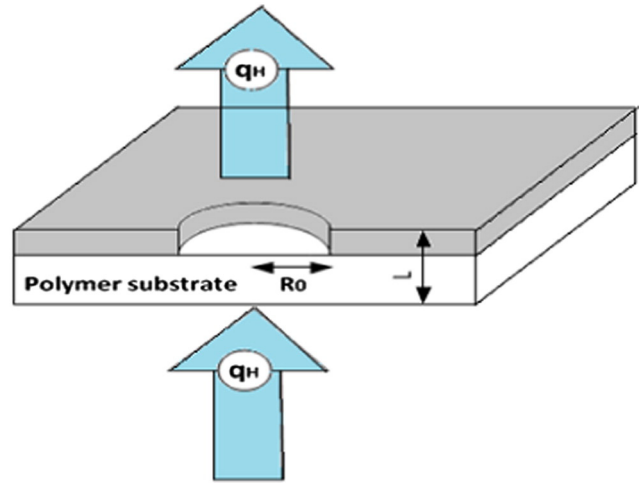


Fig. 1. A schematic representation of a hole type defect in a coated barrier film.

hole in the barrier film as shown in Fig. 1, the amount of permeant traversing the polymer and through the hole per unit time can be provided by modifying Eq. (3) and introducing the barrier film as having a circular "hole" area ( $\pi R_0^2$ ).

$$Q = \frac{q_H}{t} = \frac{\pi R_0^2 D \emptyset}{L} \quad (4)$$

where  $R_0$  is the hole radius,  $D$  is the diffusion coefficient of the barrier film ( $\text{cm}^2/\text{s}$ ),  $\emptyset$  is the water vapour concentration ( $\text{g/cm}^3$ ) and  $L$  is the combined film thickness. However, to determine the rate of the water vapour that penetrates hole over the substrate area ( $\text{g/m}^2/\text{day}$ ), Eq. (4) can be expressed as the following [24];

$$\text{WVTR} = \frac{Q}{A} \quad (\text{g/m}^2/\text{day}) \quad (5)$$

where  $Q$  is the amount of the water vapour passing through a film of thickness  $L$  and area  $A$  during time  $t$  driven by a partial pressure differential  $P$  across the film [23].

### 2.2. Case of many defects

Independent holes assume that the presence of one does not affect water vapour permeation through the other, so that their respective quantities of water vapour permeation are additive [27]. So far, a theoretical model to determine the amount of the water vapour per unit of time, traversing a single hole in a barrier coating has been assumed and in order to discuss water vapour permeation through a barrier coating containing numerous defects (holes), Eq. (5) can be modified for ( $N$ ) holes as follows:

$$\text{WVTR} = \sum_0^N \left( \frac{Q}{A} \right) N \quad (6)$$

$N$ , is the number of defects (holes) in the sample area.

## 3. Experimental details

The experimental study was based on a set of two 80 mm diameter samples. These two samples were supplied by the Centre for Process Innovation (CPI), and were coded as 2705 and 2706. These two samples are coated with 40 nm of  $\text{Al}_2\text{O}_3$  using ALD technique [28]. The ALD depositions were made using Oxford Instruments FlexAL tool, where trimethyl aluminium was used as the metal precursor [29]. The reactor temperature used to deposit the aluminium oxide was  $120^\circ\text{C}$  and the

pressure was very low (<0.1 mbar). 312 reaction cycles were induced to produce 40 nm Al<sub>2</sub>O<sub>3</sub> layers on a polyethylene naphthalate (PEN) substrate.

The Al<sub>2</sub>O<sub>3</sub> transparent ceramic material has an effective WVTR of less than  $5 \times 10^{-6}$  g/m<sup>2</sup>/day [1]. The base film substrate used in this study was PEN material; where the thickness of this substrate is specified to be 125 μm. According to the manufacturer's data, this material has a water vapour diffusion coefficient of  $4 \times 10^{-12}$  cm<sup>2</sup>/s at 38 °C, and WVTR of 4 g/m<sup>2</sup>/day at 38 °C and 90% RH. Prior to the surface measurements, the Al<sub>2</sub>O<sub>3</sub> ALD samples were measured for WVTR using isostatic standard test (Aquatrán1-MOCON®) instrumentation [30] at 38 °C and 90% RH. The lower detection limit of the instrument is  $4 \times 10^{-4}$  g/m<sup>2</sup>/day, and the uncertainty of the measurements is  $2 \times 10^{-4}$  g/m<sup>2</sup>/day for the calibration offset and  $2 \times 10^{-4}$  g/m<sup>2</sup>/day for the actual measurement, giving a total of  $4 \times 10^{-4}$  g/m<sup>2</sup>/day.

The water vapour permeation test results show that sample coded 2705 had a WVTR of  $4.1 \times 10^{-3}$  g/m<sup>2</sup>/day and sample 2706 had a WVTR of  $2.0 \times 10^{-3}$  g/m<sup>2</sup>/day (the WVTR for sample 2705 is twice as high as the WVTR for sample 2706). The WVTR results were obtained after a stabilisation time of 5 days.

#### 4. Surface topography analysis

##### 4.1. Surface topography analysis and result discussion

Surface metrology and characterisation technologies used in the present study include white light scanning interferometry (WLSI) and environmental scanning electron microscopy (ESEM) and both were applied to analyse the PV barrier film defects. It should be noted that the WLSI technique employed, imposed a lateral resolution limit on the surface measurement of ~0.88 μm. In the study quantitative surface measurement was carried out using optical interferometry and the topography was characterised using areal parameters [31]. The proportion of the surface area characterised was 14% of the total area of each sample equating to 703 mm<sup>2</sup>; this comprised 700 measurements per sample. Initially, standard statistical field parameters [32,33] in particular the root mean square surface roughness deviation ( $S_q$ ) [33] were calculated for the overall 3D surface data (defective and non-defective) in an attempt to investigate any correlations between the surface topography measurement and the WVTR. This amplitude parameter can give information regarding the areal height deviation of the surface topography for each sample, and it is defined as the root mean square value of the surface departures  $z(x, y)$ , within a sampling area [33], and is given by the following equation:

$$S_q = \sqrt{\frac{1}{MN} \sum_{j=1}^N \sum_{i=1}^M \eta^2(x_i, y_j)} \quad (7)$$

where M is a number of points per profile, N is the number of profiles and  $\eta(x_i, y_j)$  is the residual surface obtained by subtracting the reference plane from the original surface.

Applying this method to the recorded 3D surface data, the results in Fig. 2 which represent the mean value of the surface roughness for the samples showed no real differences or correlations between the studied samples other than a greater spread of root mean square roughness values for sample 2705 (high WVTR) as represented by error bars. This result seems to strongly agree with previous published work [15], where the authors observed that no correlation exists when the surface roughness is measured over large scanned areas owing to the inhomogeneous coating morphology [15].

The results shown in Fig. 2 show no clear correlation between the mean  $S_q$  value taken over the measured area of the samples and the WVTR. It can be seen that the mean  $S_q$  values are similar for both samples, while the WVTR is substantially different. Following this initial analysis only data files with defects (peaks and holes) were selected for further

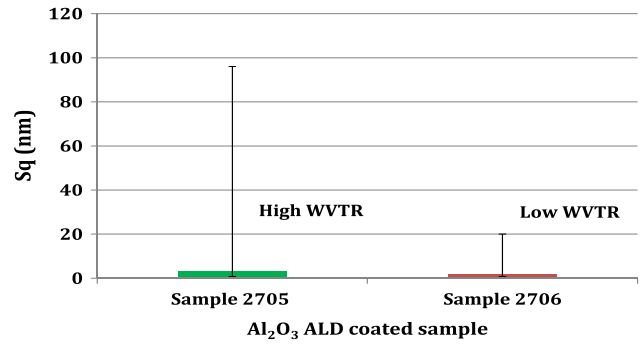


Fig. 2. The calculated mean surface roughness ( $S_q$ ) over 700 measurements for two similar samples (the error bars represent the maximum and the minimum  $S_q$  values obtained).

investigation in an attempt to investigate such correlation between defect size, density, distribution and morphology. Fig. 3 shows the number of data files with defects present on the surfaces, where each data file represents 1 mm<sup>2</sup> of the total measured area of 703 mm<sup>2</sup>.

The results in Fig. 3 indicate that sample 2706 has higher defect density than sample 2705. However, the question remains here why does sample 2706 still show lower WVTR although it has a higher defect density?

At this point, segmentation analysis [31] was carried out on the surface topography data (areas with defects present) of the samples in Fig. 3 in order to try to extract and quantify only the significant defects present on the substrate. In the present work it is postulated that only geometrically significant defects are directly responsible for the high WVTR. This method of analysis (segmentation) allows the extraction of information pertaining to specific "significant" topographical features from the topography data using a series of mathematical and thresholding techniques [31,32]. In the present case a significance value of  $\pm 3 S_q$  vertical height [where,  $S_q$  for non-defective sample area = 0.8 nm, see Fig. (4a)] and 15 μm (based on SEM analysis) lateral size was applied to compare the presence of significant defects on both samples.

Wolf pruning and area pruning [31,34] are implemented for extracting the features of functional interest by accurately excluding insignificant geometrical features, such as measurement noise and error and small topographical features. As a starting point, this method was applied to count only defects where the scale is greater than the background surface roughness variation over the total measured area. In the present case defects are assumed to manifest themselves as both negative topographical features (holes) and positive features (particulates) as shown in Fig. 5, where the particulates are considered as a defect. Zhang et al. [9] stated that particulates may be dislodged post coating or provide shadowing thus resulting in areas of uncoated substrate.

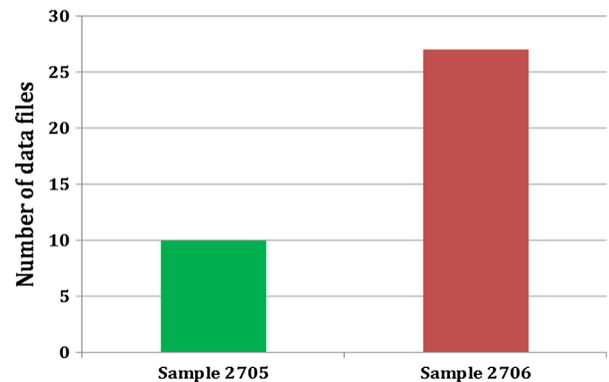


Fig. 3. Number of data files with defective regions for the two similar samples (defects defined as holes or peaks).

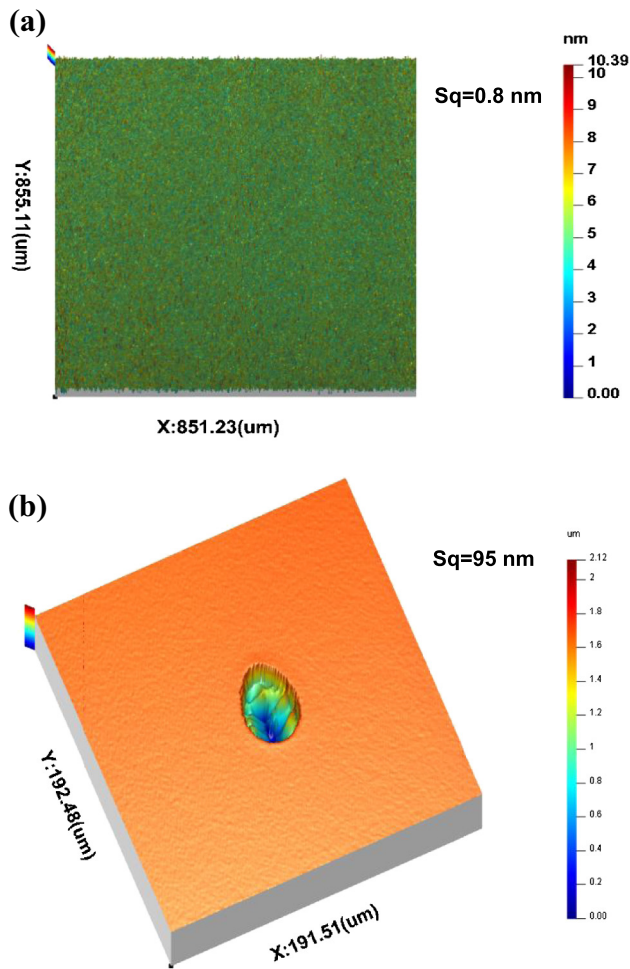


Fig. 4. Surface topography for (a) non-defective area and (b) defective area of a sample. (Note difference in  $S_q$  value).

Using the criteria outlined above ( $\pm 3 S_q$  vertical and  $15 \mu\text{m}$  lateral) it was possible to segment the surface data and record the defect density/count across the surface data sets collected from the  $\text{Al}_2\text{O}_3$  ALD coated barrier layers. Fig. 6 shows significant defect count at  $\pm 3 S_q$  vertical and  $15 \mu\text{m}$  lateral pruning conditions.

The analysis of the results in Fig. 6 showed that there was evidence of correlation between the number of large defects and the WVTR value. The high WVTR specimen (2705) had a larger density of significant defects as compared to the better performing substrate (2706). This result seems to agree with previous published work [35], which stated that large defects may dominate the permeation properties of the barrier film. However, even for sample (2706) there are still circa four significant defects affecting the barrier performance by allowing water vapour ingress. The question that remains is, are larger defects more significant in terms of WVTR and what is the cut off level between large significant defects and small insignificant defects in the present case?

Hence to investigate the lower limit of the defect size that is potentially significant, different area pruning conditions were applied while the height prune condition of  $\pm 3 S_q$  remained the same, Fig. 6. Using these criteria (different width pruning and  $\pm 3 S_q$  height), the defect density count appeared to converge around  $2.5 \mu\text{m}$  (lateral dimension) as shown in Fig. 7. However, when larger pruning values are used to define significance, the defect density level was consistently higher for the sample with the higher WVTR (2705) and from approximately  $5 \mu\text{m}$  down to  $1 \mu\text{m}$ ; the defect density count remained stable. Interpretation of the data suggests that, for defects less than  $1 \mu\text{m}$  and up to  $2.5 \mu\text{m}$  size, sample 2706 shows a higher defect density at  $\sim 24/\text{mm}^2$  while the defect

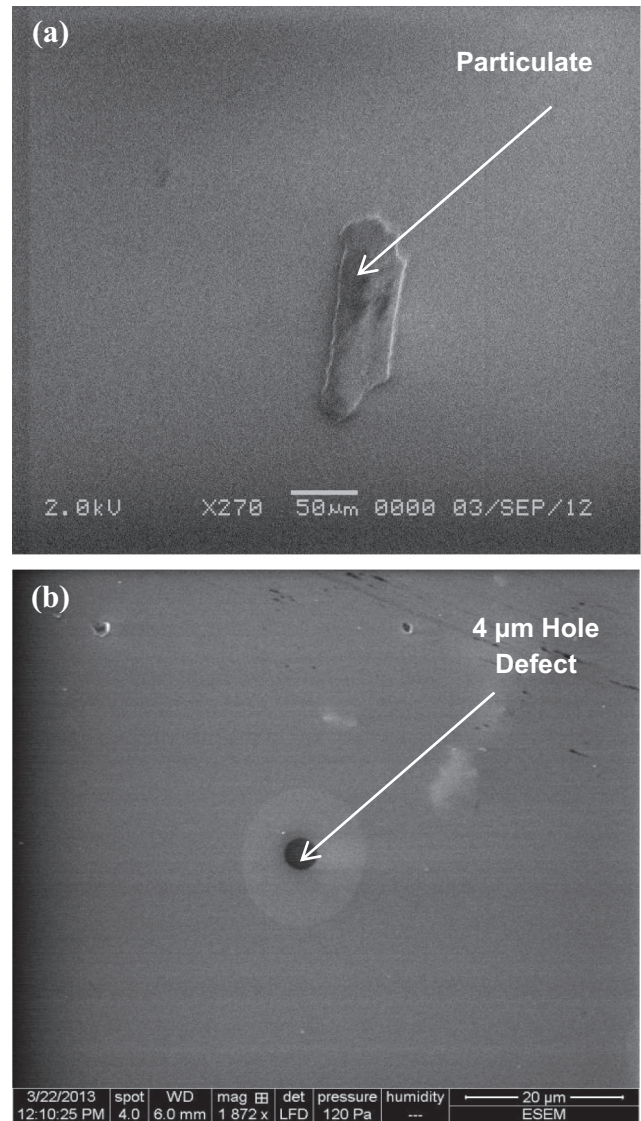


Fig. 5. Shows (a) particulate type defect, (b) hole type defect in the  $\text{Al}_2\text{O}_3$  barrier coating (ESEM images).

density for sample 2705 remains stable at  $17/\text{mm}^2$ . Above  $2.5 \mu\text{m}$ , the decreased defect density for sample 2706 throughout is highly significant. This result indicates that the sample with higher density of defects  $> 3 \mu\text{m}$  exhibits inferior barrier properties.

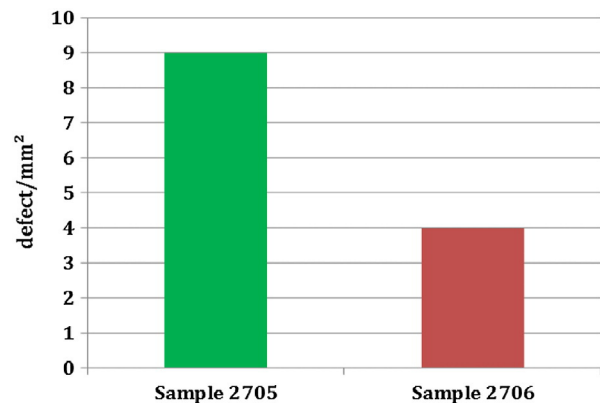


Fig. 6. Defects density at ( $\pm 3 S_q$  vertical and  $15 \mu\text{m}$  lateral) pruning conditions for the two similar samples.

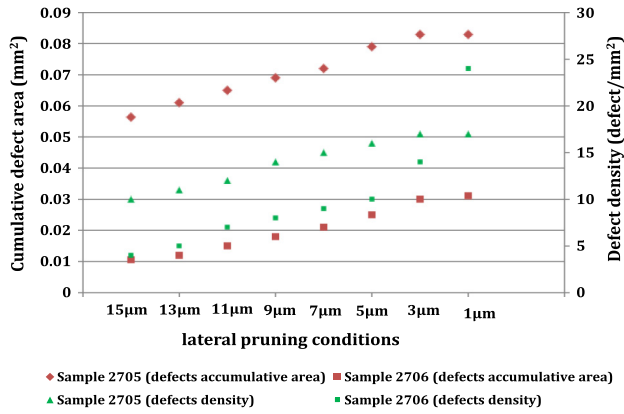


Fig. 7. Defects count and accumulative area at different lateral pruning conditions for the measured area (703 mm<sup>2</sup>) of two similar samples.

Moreover, Fig. 7 also shows a plot of the accumulated surface area of the defects measured on the two samples. The results show that when all defects with lateral widths down to 1 µm are used in the analysis, sample 2705 (high WVTR) consistently has a higher cumulative surface area value, but accompanied by a lower defect density. Consequently the results would indicate that when developing a metrology technology for defect characterisation on these types of barrier coatings only significant defects need to be quantified. Based on the results in Fig. 7, it is possible now to classify the defects in terms of their size in relation to their significance. (See table 1.)

4.2. WVTR analysis and results discussion

The cumulative defect area (over a total measured area of 703 mm<sup>2</sup>) for samples 2705 and 2706 were found to be 0.083 mm<sup>2</sup> and 0.03 mm<sup>2</sup> respectively, as shown in Fig. 7. If a homogenous distribution of the defects is assumed across the whole of the sample area (5024 mm<sup>2</sup>), then the cumulative defect areas may be scaled up linearly and are found to be 0.012% and 0.004% of the total sample area. This should result in WVTRs of  $4.86 \times 10^{-4}$  g/m<sup>2</sup>/day and  $1.65 \times 10^{-4}$  g/m<sup>2</sup>/day respectively, based on the ideal values of the WVTR for the Al<sub>2</sub>O<sub>3</sub> material (see Section 3). The experimental WVTRs of the samples, taken after a stabilisation time of 5 days, were found to be  $4.1 \times 10^{-3}$  g/m<sup>2</sup>/day (sample 2705) and  $2 \times 10^{-3}$  g/m<sup>2</sup>/day (sample 2706). Consequently using this method (the ratio of the defective area to non-defective area) does not give reliable results for quantifying the water vapour permeation through the samples, see Fig. 8. However, when referring back to the theoretical model presented earlier in the paper and using Eqs. (5) and (6) for the given sets of parameters and variables for each sample, as shown in Appendix A(1), and substituting all the known data (sample area, sample thickness, number of defects, diffusion coefficient, water vapour concentration and the accumulative area of the defects) into Eq. (6), the theoretical model based on the approach of Da Silva Sobrinho et al. [11] led to results which are similar to those obtained by surface topography analysis [36,37] and experimental WVTR test results. Calculations are shown in Appendix A(1).

Table 1  
Type and size of significant/non-significant defects in the Al<sub>2</sub>O<sub>3</sub> barrier film.

Type of defect	Feature size	
	Vertical	Lateral
Significant (holes and particulates)	≥ (±2.4) nm/field of view	≥ 3 µm lateral dimension
Non-significant (holes and particulates)	≤ (±2.4) nm/field of view	≤ 3 µm lateral dimension

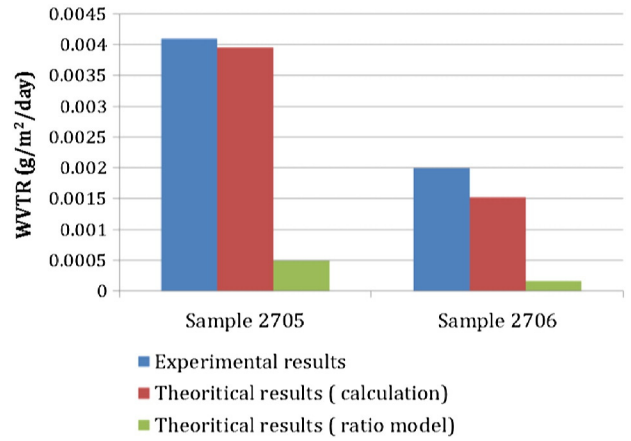


Fig. 8. Comparison between the theoretical and experimental results for the two similar samples.

The results in Fig. 8 indicate that sample 2705 has a higher WVTR value than sample 2706. This result is similar to that obtained experimentally using water vapour permeation test in Section 3. This would seem to indicate that the theoretical model presented in this paper after Da Silva Sobrinho et al. [11] has the potential to be used for understanding the mechanism of water vapour permeation through flexible PV barrier film defects.

To summarise, this investigation for the conditions studied here has shown that the total permeation rate through small numbers of larger defects is much greater than the total permeation rate through large numbers of small pinhole-type defects over the same area of substrate and that the use of a theoretical model yields similar results.

5. Conclusion

The segmentation analysis results and the theoretical model approach in this research paper, both appear to indicate that the major contributing factor for determining the WVTR is the total number of larger defects, where the sample with higher density of defects > 3 µm exhibit inferior barrier properties. The model presented in this paper could therefore also be used for the understanding of the overall PV module efficiency, performance and lifespan. In addition to this, the results would seem to indicate that, for these substrates produced under the stated conditions, the critical spatial resolution required for defect detection need not be less than 3 µm, as any defect that has less than this lateral size seems to have a much lower effect on the barrier properties.

Acknowledgements

The authors would like to thank the EU for providing funds to carry out this work via the NanoMend project NMP4 LA-2011-280581, the EPSRC Centre for Innovative Manufacturing in Advanced Metrology (EP/I033424/1), and the Libyan Cultural Attaché in London (EE178-522-30836 (2013/2014)).

Appendix A

Sample 2705 data		
Parameter	Given unit	Metric unit (m)
L (film thickness)	125.04 µm	0.000125 m
D (diffusion coefficient)	$4 \times 10^{-12}$ cm <sup>2</sup> /s	$4 \times 10^{-16}$ m <sup>2</sup> /s
∅ (water vapour concentration)	1 g/cm <sup>3</sup>	1,000,000 g/m <sup>3</sup>
Accumulated defect area (A)	0.592558 mm <sup>2</sup>	$5.93 \times 10^{-7}$ m <sup>2</sup>
Sample area (A)	5024 mm <sup>2</sup>	m <sup>2</sup> 0.00524
N (total number of defects at 3 µm)	121	121

$$Q(\text{one hole}) = \frac{q_H}{t} = \frac{\pi R_0^2 D \Delta}{L}$$

$$Q(\text{many holes}) = \frac{q_H}{t} = \frac{A_{\text{cumulative}} D \Delta}{L}$$

$$Q = \frac{5.93 \times 10^{-7} \times 4 \times 10^{-16} \times 1 \times 10^6}{0.000125} = 1.90 \times 10^{-12} \text{ g/s.}$$

$$\text{WVTR} = \frac{Q}{A} \times N \times 86400(\text{day}).$$

$$\text{WVTR} = \frac{1.90 \times 10^{-12}}{0.00524} \times 121 \times 86400 = 3.96 \times 10^{-3}.$$

$$\text{WVTR} = 3.96 \times 10^{-3} \text{ g/m}^2/\text{day}.$$

Sample 2706 data		
Parameter	Given unit	Metric unit (m)
L (film thickness)	125.04 $\mu\text{m}$	0.000125 m
D (diffusion coefficient)	$4 \times 10^{-12} \text{ cm}^2/\text{s}$	$4 \times 10^{-16} \text{ m}^2/\text{s}$
$\Delta$ (water vapour concentration)	1 $\text{g}/\text{cm}^3$	1,000,000 $\text{g}/\text{m}^3$
Accumulated defect area (A)	0.2003 $\text{mm}^2$	$2.003 \times 10^{-7} \text{ m}^2$
Sample area (A)	5024 $\text{mm}^2$	$\text{m}^2$ 0.00524
N (total number of defects at 3 $\mu\text{m}$ )	136	136

$$Q(\text{one hole}) = \frac{q_H}{t} = \frac{\pi R_0^2 D \Delta}{L}$$

$$Q(\text{many holes}) = \frac{q_H}{t} = \frac{A_{\text{cumulative}} D \Delta}{L}$$

$$Q = \frac{2.003 \times 10^{-7} \times 4 \times 10^{-16} \times 1 \times 10^6}{0.000125} = 6.82 \times 10^{-13} \text{ g/s.}$$

$$\text{WVTR} = \frac{Q}{A} \times N \times 86400(\text{day}).$$

$$\text{WVTR} = \frac{6.41 \times 10^{-13}}{0.00524} \times 136 \times 86400 = 1.53 \times 10^{-3}.$$

$$\text{WVTR} = 1.53 \times 10^{-3} \text{ g/m}^2/\text{day}.$$

## References

- [1] P.F. Carcia, R.S. McLean, S. Hegedus, ALD moisture barrier for Cu (InGa) Se<sub>2</sub> solar cells, ECS Trans. 33 (2010) 237.
- [2] M. Igalson, A. Urbaniak, Defect states in the CIGS solar cells by photocapacitance and deep level optical spectroscopy, Technol. Sci. 53 (2005) 157.
- [3] IEC 61646, Thin-film Terrestrial Photovoltaic (PV) Modules—Design, Qualification and Type Approval, second ed. IEC Central Office, Geneva, 2008.
- [4] D.J.L. Br , Investigation and development of CIGS solar cells on flexible substrates and with alternative electrical back contacts, Diss., Eidgenossische Technische Hochschule ETH Z rich, Zurich, 2009.
- [5] M.D. Kempe, Control of moisture ingress into photovoltaic modules, Photovoltaic Specialists Conference. Conference Record of the Thirty-first IEEE, 2005, p. 503.
- [6] A.A. Dameron, S.D. Davidson, B.B. Burton, P.F. Carcia, R.S. McLean, S.M. George, Gas diffusion barriers on polymers using multilayers fabricated by Al<sub>2</sub>O<sub>3</sub> and rapid SiO<sub>2</sub> atomic layer deposition, J. Phys. Chem. C 112 (2008) 4573.
- [7] J.H. Hotchkiss, Food-packaging interactions influencing quality and safety, Food Addit. Contam. 14 (1997) 601.
- [8] M. Chainey, Transport phenomena in polymer films, in: N.P. Cheremisinoff (Ed.), Handbook of Polymer Science and Technology, Marcel Dekker, Inc., New York, 1989, p. 499.
- [9] Y. Zhang, Y.-Z. Zhang, D.C. Miller, J.A. Bertrand, S.-H. Jen, R. Yang, M.L. Dunn, S.M. George, Y. Lee, Fluorescent tags to visualize defects in Al<sub>2</sub>O<sub>3</sub> thin films grown using atomic layer deposition, Thin Solid Films 24 (2009) 6794.
- [10] Y. Zhang, J.A. Bertrand, R. Yang, S.M. George, Y. Lee, Electroplating to visualize defects in Al<sub>2</sub>O<sub>3</sub> thin films grown using atomic layer deposition, Thin Solid Films 11 (2009) 3269.
- [11] A. da Silva Sobrinho, G. Czeremuskin, M. Latreche, M. Wertheimer, Defect-permeation correlation for ultrathin transparent barrier coatings on polymers, J. Vac. Sci. Technol. A 18 (2000) 149.
- [12] H. Chatham, Oxygen diffusion barrier properties of transparent oxide coatings on polymeric substrates, Surf. Coat. Technol. 78 (1996) 1.
- [13] M. Hanika, H.C. Langowski, U. Moosheimer, W. Peukert, Inorganic layers on polymeric films—influence of defects and morphology on barrier properties, Chem. Eng. Technol. 26 (2003) 605.
- [14] A. Erlat, R. Spontak, R. Clarke, T. Robinson, P. Haaland, Y. Tropsha, N. Harvey, E. Vogler, SiO<sub>x</sub> gas barrier coatings on polymer substrates: morphology and gas transport considerations, J. Phys. Chem. B 103 (1999) 6047.
- [15] G. Garcia-Ayuso, L. Vázquez, J.M. Mart nez-Duart, Atomic force microscopy (AFM) morphological surface characterization of transparent gas barrier coatings on plastic films, Surf. Coat. Technol. 80 (1996) 203.
- [16] A.G. Erlat, B.M. Henry, C.R. Grovenor, A.G. Briggs, R.J. Chater, Y. Tsukahara, Mechanism of water vapor transport through PET/AIO<sub>x</sub> N<sub>y</sub> gas barrier films, J. Phys. Chem. B 108 (2004) 883.
- [17] J.S. Lewis, M.S. Weaver, Thin-film permeation-barrier technology for flexible organic light-emitting devices, IEEE J. Sel. Top. Quantum Electron. 10 (2004) 45.
- [18] A. Ruanthong, C. Thanachayanont, T. Sarakonsri, Preparation of CIGS p-type semiconductor used as thermoelectric material by sol-gel, J. Mater. Sci. Appl. Energy 3 (2013) 10.
- [19] W. Henry, Experiments on the quantity of gases absorbed by water, at different temperatures, and under different pressures, Philos. Trans. R. Soc. London, Ser. A 93 (1803) 29.
- [20] A. Fick, Ueber diffusion, Ann. Phys. 170 (1855) 59.
- [21] W. Su-Huai, S.B. Zhang, A. Zunger, Effects of Ga addition to CuInSe<sub>2</sub> on its electronic, structural, and defect properties, Appl. Phys. Lett. 72 (1998) 3199.
- [22] S.v. Wroblewski, Ueber die Natur der Absorption der Gase, Ann. Phys. 244 (1879) 29.
- [23] R. Ashley, Permeability and plastics packaging, in: J. Comyn (Ed.), Polymer Permeability, Chapman & Hall, London, 1985, p. 269.
- [24] F. Debeaufort, A. Voilley, P. Meares, Water vapor permeability and diffusivity through methylcellulose edible films, J. Membr. Sci. 91 (1994) 125.
- [25] M. Kanezashi, T. Tsuru, Gas permeation properties of helium, hydrogen, and polar molecules through microporous silica membranes at high temperatures: correlation with silica network structure, in: S.T. Oyama, S.M. Stagg-Williams (Eds.), Inorganic, Polymeric and Composite Membranes: Structure, Function and Other Correlations, Elsevier, Oxford, 2011, p. 117.
- [26] J.A. Bertrand, D.J. Higgs, M.J. Young, S.M. George, H<sub>2</sub>O vapor transmission rate through polyethylene naphthalate polymer using the electrical Ca test, J. Phys. Chem. A 117 (2013) 12026.
- [27] A.S. Da Silva Sobrinho, M. Latreche, G. Czeremuskin, J.E. Klemberg-Sapieha, M.R. Wertheimer, Transparent barrier coatings on polyethylene terephthalate by single- and dual-frequency plasma-enhanced chemical vapor deposition, J. Vac. Sci. Technol. A 16 (1998) 3190.
- [28] S.M. George, Atomic layer deposition: an overview, Chem. Rev. 110 (2009) 111.
- [29] S.M. George, B. Yoon, A.A. Dameron, Surface chemistry for molecular layer deposition of organic and hybrid organic-inorganic polymers, Acc. Chem. Res. 42 (2009) 498.
- [30] B. Duncan, J. Urquhart, S. Roberts, Review of measurement and modelling of permeation and diffusion in polymers, NPL Report DEPC MPR 012. Middlesex, 2005, p. 1.
- [31] ISO 25178, Geometrical Product Specifications (GPS)—Surface Texture: Areal—Part 2: Terms, Definitions and Surface Texture Parameters, first ed. International Organization for Standardisation, Geneva, 2012.
- [32] L. Blunt, X. Jiang, Numerical parameters for characterisation of topography, in: L. Blunt, X. Jiang (Eds.), Advanced Techniques for Assessment Surface Topography: Development of a Basis for 3D Surface Texture Standards “Surfstand”, Kogan Page Science, London, 2003, p. 17.
- [33] K.J. Stout, L. Blunt, Three Dimensional Surface Topography, second ed. Elsevier, London, 2000.
- [34] X. Jiang, P.J. Scott, D. Whitehouse, L. Blunt, Paradigm shifts in surface metrology. Part II. The current shift, Proc. R. Soc. London, Ser. A 463 (2007) 2071.
- [35] A. Erlat, B. Henry, J. Ingram, D. Mountain, A. McGuigan, R. Howson, C. Grovenor, G. Briggs, Y. Tsukahara, Characterisation of aluminium oxynitride gas barrier films, Thin Solid Films 388 (2001) 78.
- [36] L. Blunt, M. Elrawemi, L. Fleming, F. Sweeney, Correlation of micro and nano-scale defects with WVTR for aluminium oxide barrier coatings for flexible photovoltaic modules, Int. J. Precis. Technol. 3 (2013) 290.
- [37] M. Elrawemi, L. Blunt, L. Fleming, F. Sweeney, Further development of surface metrology methods for predicting the functional performance of flexible photovoltaic barrier films, Surf. Topogr. Metrol. Prop. 1 (2013) 015006.